Geoscience Frontiers 16 (2025) 102045

Contents lists available at ScienceDirect

Geoscience Frontiers

journal homepage: www.elsevier.com/locate/gsf

Research Paper

Assessment of trace elements distribution and sources from snowpits in the Lambert Glacier region, coastal East Antarctica

Yalalt Nyamgerel [a], Soon Do Hur [b], Tseren-Ochir Soyol-Erdene [c], Cunde Xiao [d], Hyejung Jung [a], Jeonghoon Lee [a,*]

[a] Department of Science Education, Ewha Womans University, Seoul 120-750, Republic of Korea
[b] Division of Glacier and Earth Sciences, Korea Polar Research Institute, Incheon 21990, Republic of Korea
[c] Department of Green Energy and Engineering, School of Engineering and Technology, National University of Mongolia, Ulaanbaatar 14201, Mongolia
[d] State Key Laboratory of Earth Surface Processes and Resource Ecology, Beijing Normal University, Beijing 100875, China

ARTICLE INFO

Article history:
Received 31 October 2024
Revised 17 February 2025
Accepted 31 March 2025
Available online 4 April 2025
Handling Editor: Yirang Jang

Keywords:
Trace elements
Spatial variation
Antarctica
Lambert Glacier Basin
Positive matrix factorization

ABSTRACT

The measurement of trace elements in Antarctic snow is crucial for understanding historical atmospheric geochemical changes and circulation patterns. However, studies on their spatial distributions remain limited, particularly those evaluating multiple metals across several snowpits, making interpretation challenging. This study investigates the distributions and sources of trace elements—including Cd, Ba, Pb, U, Bi, V, Mn, Fe, Cu, Zn, and As—across four snowpits in the Lambert Glacier Basin, East Antarctica. The trace elements exhibit site-, element-, and season-dependent variations, with higher concentrations observed at inland sites. In contrast, $\delta^{18}O$ and ion concentrations decrease with increasing distance from the coast and elevation, underscoring the influence of marine emissions. Crustal sources primarily contributed to Ba, U, V, Mn, and Fe, while non-crustal sources predominantly contributed to Cd, Bi, Zn, Pb, Cu, and As. Positive matrix factorization (PMF) analysis indicates that trace element concentrations in Pits 2 and 3 are influenced by both crustal and non-crustal sources, while Pit 4 reflects a mixed-source influence. Pit 1 (coastal site) also indicates the mixed sources with influence of a highly dynamic marine climate and environment. The PMF results reveal similarities in emission sources and atmospheric transport patterns across the snowpits, facilitating a more comprehensive interpretation of longer ice core records. Overall, this study provides valuable insights into trace element distributions and enhances our understanding of past environmental and climatic conditions.

© 2025 China University of Geosciences (Beijing) and Peking University. Published by Elsevier B.V. on behalf of China University of Geosciences (Beijing). This is an open access article under the CC BY-NC-ND license (http://creativecommons.org/licenses/by-nc-nd/4.0/).

1. Introduction

Antarctica is regarded as one of the most pristine environments, making the study of trace elements in Antarctic snow crucial for understanding historical changes in atmospheric geochemical composition and circulation patterns (Gabrielli et al., 2010; Hong et al., 2013). Therefore, identifying the transport and deposition patterns of trace elements in Antarctic snow, along with their local, regional, and global sources, is essential. To date, several studies have reported various emission sources of trace elements, including crustal dust, marine aerosols, volcanic activity, and anthropogenic influences (Barbante et al., 1998; Van de Velde et al., 2005; Dixon et al., 2013; Sayyed, 2014; Shi et al., 2015; Marchant et al., 2017; Jiang et al., 2018; Liu et al., 2021). While the emission intensity of trace elements is primarily driven by wind strength (Gabrielli et al., 2009; Hong et al., 2013; Tuohy et al., 2015; Zheng et al., 2021), atmospheric circulation also plays a pivotal role in their transport and deposition (Fischer et al., 2017).

Lambert Glacier, the largest outlet glacier in Antarctica, is a key site for studying ice sheet dynamics and climate change (Tang et al., 2020). Numerous studies have examined the spatial distribution of various trace elements in surface snow samples along the transect from Lambert Glacier to the Dome A site (Li et al., 2014; Li et al., 2016; Jiang et al., 2018; Du et al., 2019; Herath et al., 2024). These studies suggest that trace element concentrations in the region are influenced by multiple potential sources and transporting air masses. Local atmospheric transport is considered more significant for ice core climate signals in this area than large-scale or global circulation patterns (Xiao et al., 2004). Additionally,

* Corresponding author.
E-mail address: jeonghoon.d.lee@gmail.com (J. Lee).

https://doi.org/10.1016/j.gsf.2025.102045
1674-9871/© 2025 China University of Geosciences (Beijing) and Peking University. Published by Elsevier B.V. on behalf of China University of Geosciences (Beijing). This is an open access article under the CC BY-NC-ND license (http://creativecommons.org/licenses/by-nc-nd/4.0/).

substantial regional variations in trace element distribution have been observed near the Lambert Glacier Basin (Xiao et al., 2004). These variations are controlled by the sources, transport pathways, and deposition patterns of the elements rather than the region's proximity to the coast or altitude (Jiang et al., 2018). However, source apportionment remains challenging, as previous studies have highlighted the complexity and inconsistency in results due to significant variations in precipitation over the open ocean (Shi et al., 2015), aerosols (Xu et al., 2019), surface snow (Jiang et al., 2018; Herath et al., 2024), and topsoil (Xu et al., 2020).

Liu et al. (2021) assessed the temporal variations in the distribution of 14 trace elements in a snowpit at Dome A, while Hur et al. (2007) examined the seasonal distributions of 11 trace elements in a single snowpit at Lambert Glacier. However, no study has yet focused on the spatial variations and sources of various trace elements across multiple snowpits in this region. The episodic and site-dependent nature of trace element distributions complicates such evaluations (Hur et al., 2007; Hong et al., 2012; Kakareka et al., 2020; Nyamgerel et al., 2024). Moreover, research on the spatial distribution of trace elements across Antarctica remains limited due to the continent's vastness. Therefore, further efforts to investigate the spatial distributions and sources of trace elements in Antarctica are crucial. In response, this study examines the spatial distributions and sources of various elements — including Al, V, Mn, Fe, Cu, As, Cd, Ba, Pb, Bi, and U — alongside water isotopes ($\delta^{18}O$) and major ions in four snowpits (Pits 1 – 4) located in the Lambert Glacier region, covering a two- to four-year period. Samples were collected along a traverse from Zhongshan Research Station to Dome A, spanning approximately 450 km from the coast. The regional distribution of these trace elements was analyzed, and

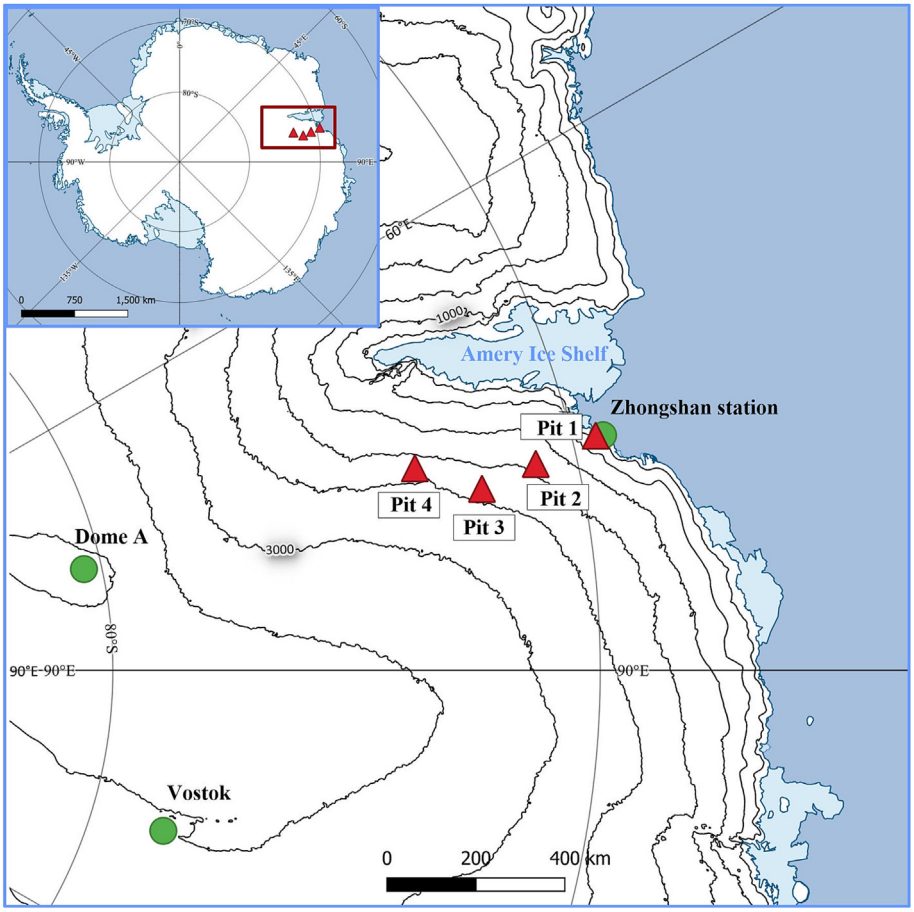


Fig. 1. Map indicating the locations of the four snow pits near Zhongshan Research Station, East Antarctica. Dome A and Vostok ice core sites are marked using green dots. This map is generated using the QGIS software using datasets obtained from the Quantarctica3 project (Matsuoka et al., 2021). (For interpretation of the references to colour in this figure legend, the reader is referred to the web version of this article.)

Table 1
Location and sampling data of the four snow pits.

	Pit 1	Pit 2	Pit 3	Pit 4
Latitude (S)	69° 31′14″	70° 50′ 07″	72° 00′ 49″	73° 15′ 00″
Longitude (E)	76° 17′ 33″	77° 04′ 29″	77° 55′ 38″	75° 29′ 59″
Altitude (m)	529	1850	2390	2215
Distance to coast (km)	~ 50	~190	~330	~450
Sampling date	January 2002	January 2002	December 2002	December 2002
Depth (cm)	125	230	170	255
Number of samples	25	47	34	51
Annual mean snow accumulation in snow depth (cm)	46.25 ± 19.45	59.17 ± 21.26	44.17 ± 11.27	51.88 ± 2.39
Period (number of full years)	1999–2002 (2)	1998–2002 (3)	1999–2002 (3)	1997–2002 (4)

potential source contributions were quantified to refine source apportionment. These findings offer valuable insights into the atmospheric distribution of these elements, supporting paleoclimatic studies based on longer ice core records.

2. Materials and methods

2.1. Study area and sampling

The Lambert Glacier, located in East Antarctica and facing the southern Indian Ocean, includes the Amery Ice Shelf, a floating ice formation in Prydz Bay (Fricker et al., 2002). Four snowpits were excavated on the eastern side (Princess Elizabeth Land) of the Lambert Glacier (Fig. 1). The mean annual surface air temperature at the weather station, which is located 160 km from the coast, is −25.6 °C (Du et al., 2020). Data from the weather station network, which extends from the coast of Prydz Bay to Dome A, indicate substantial diurnal variations in wind speed in the coastal region, with predominant wind directions from the north and east (Ding et al., 2022). Wind speeds are notably higher in winter than in summer (Tang et al., 2020; Ding et al., 2022). Oceanic moisture transport primarily affects the eastern side of the Lambert Glacier Basin, where local atmospheric circulation also plays a crucial role (Xiao et al., 2004). The annual mean snow accumulation rates on the eastern side of the Lambert Glacier Basin ranged from 131.4 to 153.3 kg m^{-2} a^{-1} between 1940 and 1997, with the moisture supply assumed to originate from the southern Indian Ocean (Xiao et al., 2004). In the four snow pits examined in this study, snow accumulation rates ranged from 45.83 to 60.83 cm in snow depth (Table 1).

During the 2001/2002 Chinese Antarctic Research Expedition, snowpits were excavated at various elevations and distances from the coast. Pit 1 was located 50 km inland, while the remaining pits

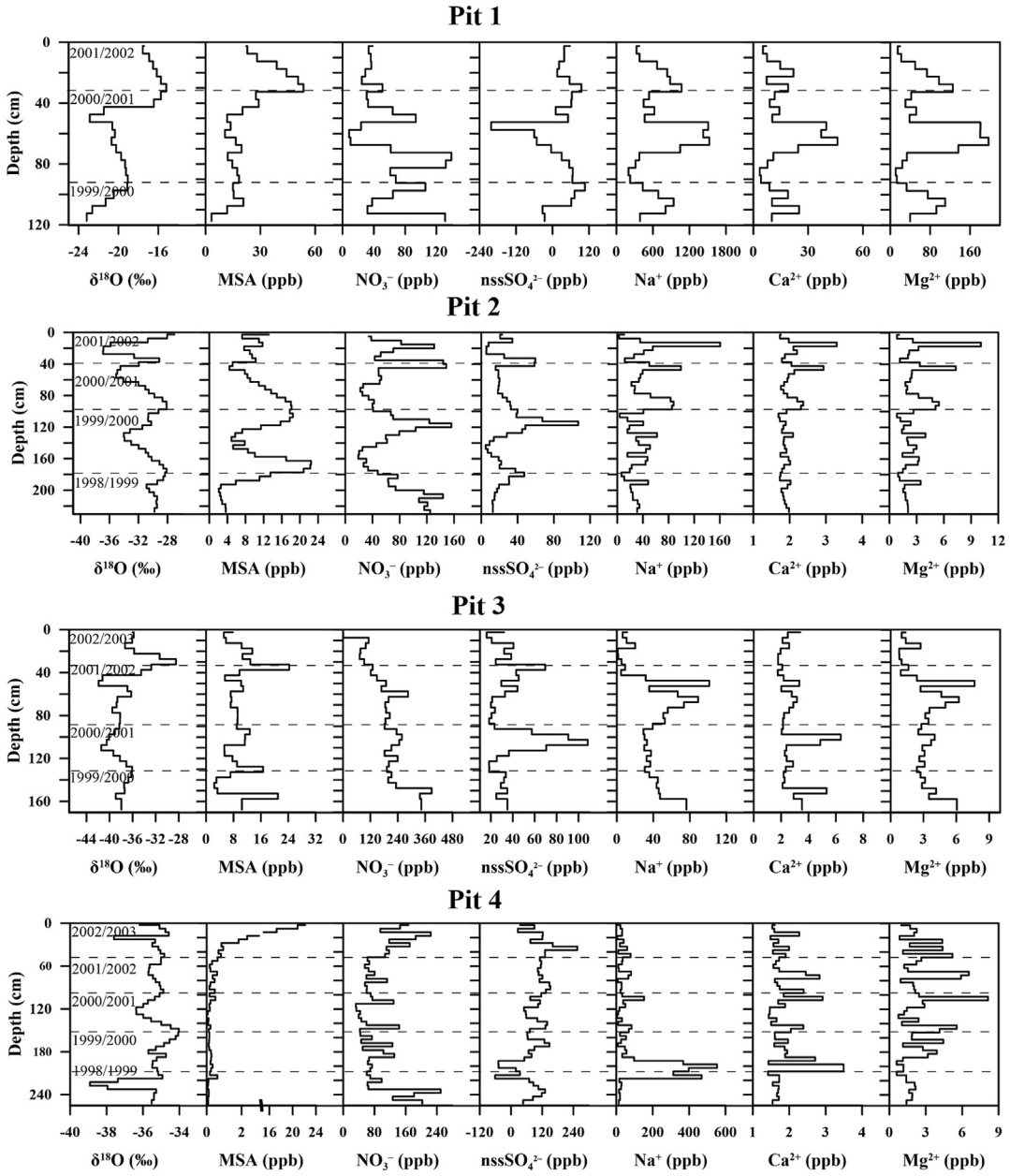


Fig. 2. Depth profiles of $\delta^{18}O$ and major ion concentrations in the four snow pits. Horizontal dash lines denote the maxima of $\delta^{18}O$ values, indicating the austral summer season.

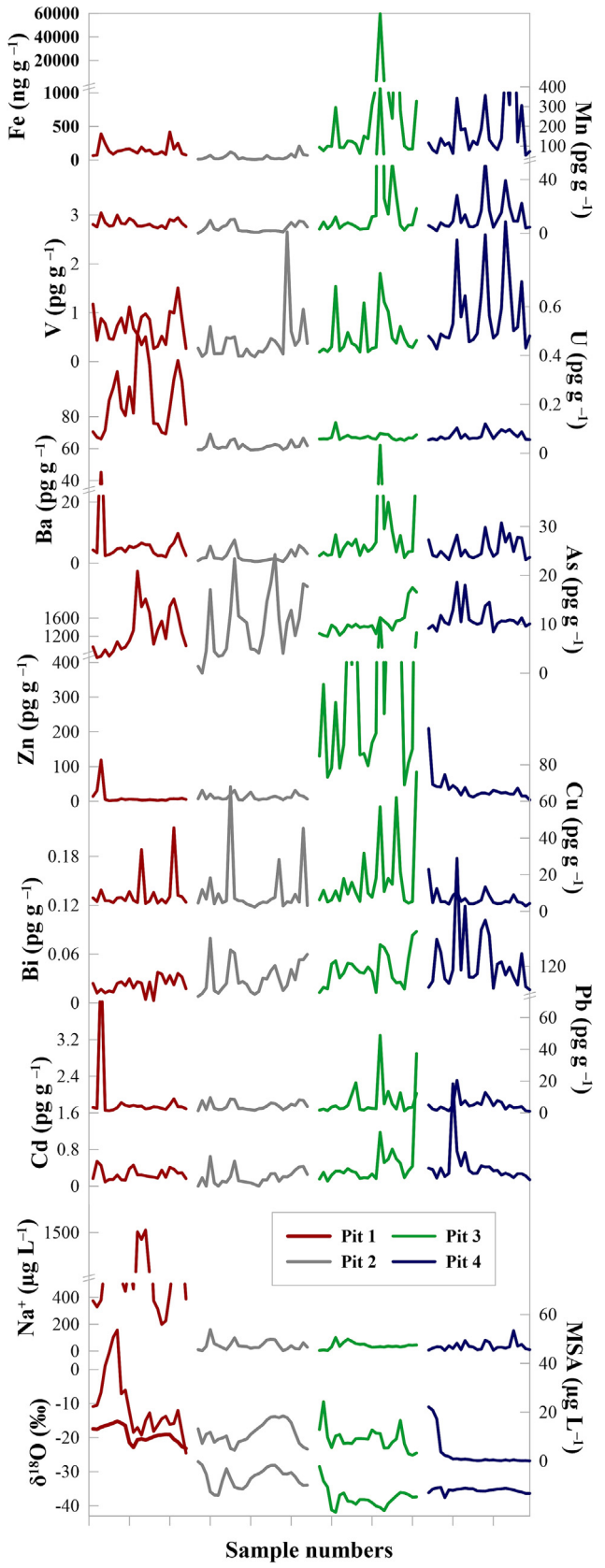


Fig. 3. Comparison of the trace element, MSA, and Na^+ concentrations, as well as $\delta^{18}O$ values, in the snowpits during the period 1999–2002. Snow pits are ordered based on their distance from the coast. The horizontal axis corresponds to the increasing depths in the snowpits.

were excavated at intervals of 120 to 140 km (Fig. 1 and Table 1). To prevent contamination, snow sampling was conducted with strict precautions. Field personnel wore cleanroom garments and polyethylene gloves and used acid-cleaned plastic shovels. Additionally, acid-cleaned ultraclean low-density polyethylene (LDPE) scrapers were used to remove approximately 10 cm of surface snow. Snow samples were collected continuously at 5-cm intervals by horizontally inserting an ultraclean cylindrical Teflon container (5 cm in diameter and 35 cm in length) into the snow. The collected snow was then transferred into ultraclean 500 mL LDPE bottles. All sampling equipment was meticulously cleaned following the protocol outlined by Hong et al. (2000a). The sample bottles were double-sealed in acid-cleaned LDPE bags and kept frozen until analysis.

2.2. Chemical analysis

Trace elements in the snow samples were analyzed at the Department of Environmental Sciences in Venice using inductively coupled plasma sector field mass spectrometry (ICP-SFMS) with an Element 2 instrument from Thermo Electron Corporation (Bremen, Germany). Sample handling and measurement procedures followed those outlined by Planchon et al. (2002). Aluminum (Al) and other major ions in the snow samples were analyzed at the Korea Polar Research Institute (KOPRI). For Al analysis, the snow samples underwent pre-concentration through non-boiling evaporation treatment (Görlach and Boutron, 1990) and were analyzed using graphite furnace atomic absorption spectrometry with a Perkin Elmer 4110ZL instrument equipped with a Zeeman background corrector (Hong et al., 2000b). Oxygen isotope ($\delta^{18}O$) measurements were conducted at the Korea Basic Science Institute using isotopic ratio mass spectrometry, achieving an analytical reproducibility of 0.1‰ (Lee et al., 2003). Meanwhile, Na, Cl, methanesulfonic acid (MSA), SO_4^{2-}, and NO_3^- were measured by ion chromatography at KOPRI using Dionex columns (AS 11 for anions and CS 14 for cations). The analytical precision for these ions ranged from 5% to 10% (Hur et al., 2007). The snowpits were dated based on seasonal peaks of $\delta^{18}O$, MSA, and NO_3^-, following the methodology recommended by Hur et al. (2007) and illustrated in Fig. 2. The age of each sample was determined by linear interpolation between consecutive $\delta^{18}O$ peaks. Due to the absence of density measurement data, snow accumulation values are reported in terms of snow depth (cm) (Table 1).

Aluminum (Al) is commonly used as a proxy for the continental crust (Rhodes et al., 2011; Schwanck et al., 2017; Liu et al., 2021). Therefore, the crustal enrichment factor (EF_c)—which represents the concentration ratio of each element relative to Al, normalized to the same ratio in the upper continental crust (Wedepohl, 1995)—was used to assess the contribution of crustal dust to the measured trace element concentrations. EF_c values below 10 indicate a crustal source, while values above 10 suggest alternative sources (Han et al., 2020). Additionally, EF_c values were calculated for select elements (Pb, Mn, Fe, Cu, Zn) based on their ratios in the local mineral composition of the Larsemann Hills (Shi et al., 2018). The contribution of marine sea-salt spray (EF_m) was determined using measured Na^+ concentrations at the same depth resolution, along with metal/Na^+ ratios obtained from surface ocean water (Lide, 2005). Volcanic contributions were assumed to be minimal in these short elemental records due to their tentative nature and the associated substantial uncertainties (Hur et al., 2007).

Pearson's correlation analysis was conducted to explore relationships between trace elements. Additionally, principal component analysis (PCA) was performed using JMP® statistical software to examine correlations and common variability within

the snowpit records (Nyamgerel et al., 2020). To further analyze the contributions of potential sources to trace element concentrations, positive matrix factorization (PMF) was applied using EPA PMF 5.0 software (https://www.epa.gov/air-research/positive-matrix-factorization-model-environmental-data-analyses) (Norris et al., 2014). PMF is a multivariate factor analysis tool that decomposes a matrix of speciated sample data into two submatrices: factor contributions (source contributions) and factor profiles (source types) (Ito et al., 2004; Rodenburg et al., 2014; Taghvaee et al., 2018; Yang et al., 2024). Compared to PCA, PMF generally offers greater stability and robustness in identifying source profiles and quantifying their contributions (Cesari et al., 2016; Liu et al., 2022). In this study, PMF analysis was conducted using 2–6 factors and 20 base runs for the input data of each snowpit, with validation through recommended bootstrap runs (100 runs) (Norris et al., 2014). The base run outputs were accepted if bootstrap mapping was available for more than 80% of the factors (Norris et al., 2014; Taghvaee et al., 2018). Based on the results, two factors were selected for Pits 2 and 3, while three factors were chosen for Pits 1 and 4.

3. Results and discussion

3.1. Distributions of $\delta^{18}O$ values, ions, and trace elements

The statistical summary of $\delta^{18}O$ and ions is shown in Supplementary Data Table S1. The mean $\delta^{18}O$ values show a gradual depletion with increasing elevation and distance from the coast (Fig. 3). Pit 3 exhibits the lowest mean $\delta^{18}O$ value (–37.36‰), with a substantial difference of 13.4‰ between the minimum and maximum values, which can be attributed to its higher elevation compared to the other pits. In contrast, ion concentrations are significantly higher in Pit 1, reflecting its proximity to the coast. These patterns are consistent with findings from a previous study (Huang et al., 2021). A gradual decrease in mean MSA concentrations is observed with increasing distance from the coast. Notably, the mean concentrations of non-sea-salt sulfates ($nssSO_4^{2-}$) are particularly high in Pits 2, 3, and 4, with Pit 4 displaying $nssSO_4^{2-}$ levels comparable to those recorded at transect locations approximately 400–500 km inland (Du et al., 2019). Inland sites (Pits 2, 3, and 4) exhibit similar concentrations of sea salt ions (Na^+, Ca^{2+}, K^+, Mg^{2+}, Cl^-, and NO_3^-), though Pit 3 shows slightly higher concentrations of Ca^{2+}, K^+, Mg^{2+}, Cl^-, and NO_3^-. Correlation analysis (results not shown) for Pit 1 reveals a positive correlation between $\delta^{18}O$ values and MSA and $nssSO_4^{2-}$ concentrations, suggesting that their abundance increases during warmer periods. However, this correlation is not observed in Pits 2, 3, and 4, indicating that Pit 1 (a coastal site) is predominantly influenced by oceanic air masses, while the other sites are likely affected by a mixture of oceanic and continental air masses.

The concentration ranges of trace elements (Supplementary Data Table S2) observed in this study are comparable to those reported in previous studies conducted in this region (Jiang et al., 2018; Du et al., 2019; Du et al., 2020) and other locations in East Antarctica, such as Law Dome, Coats Land, and Dome A (Planchon et al., 2002; Vallelonga et al., 2004; Liu et al., 2021). Notably, the concentrations of As in the snowpits are significantly higher than those observed in surface snow samples (Jiang et al., 2018), suggesting contributions from anthropogenic sources, including human activities at scientific stations and long-range atmospheric transport (Herath et al., 2024). No consistent trend is observed in the mean concentrations of trace elements with increasing distance from the coast or elevation. However, Pit 3 exhibits the highest concentrations of Cd, Ba, Mn, Fe, Cu, Zn, and As, while Pit 4 displays the second-highest concentrations of Cd, Mn, Fe, and Zn. These findings suggest that inland sites experience relatively higher metal deposition, consistent with the elevated concentrations of As, Cd, Fe, Mn, Pb, Zn, and V observed in surface snow samples (Herath et al., 2024). The increased elemental concentrations at inland locations may be attributed to differences in atmospheric transport mechanisms at each site, with additional contributions from local ice-free areas such as Vestfold Hills and Larsemann Hills.

Fig. 3 illustrates the concentration trends of trace elements between 1999 and 2002. Although no clear trend is apparent with increasing distance from the coast or changes in elevation, distinct patterns for individual metals are evident at each site. Notably, only Bi and As concentrations show a slight increasing trend. While a previous study reported an increase in lead (Pb) concentrations in surface snow samples collected along the traverse from Zhongshan Station to Dome A within 450 km of the coast (Du et al., 2019), no such trend was observed in the present study. The previous study also reported sporadic variations in vanadium (V) and cadmium (Cd) concentrations in the collected snow samples (Du et al., 2019). The discrepancies between the results of the two studies are attributed to their different study locations and the substantial variations in trace element distributions (Hur et al., 2007; Hong et al., 2012).

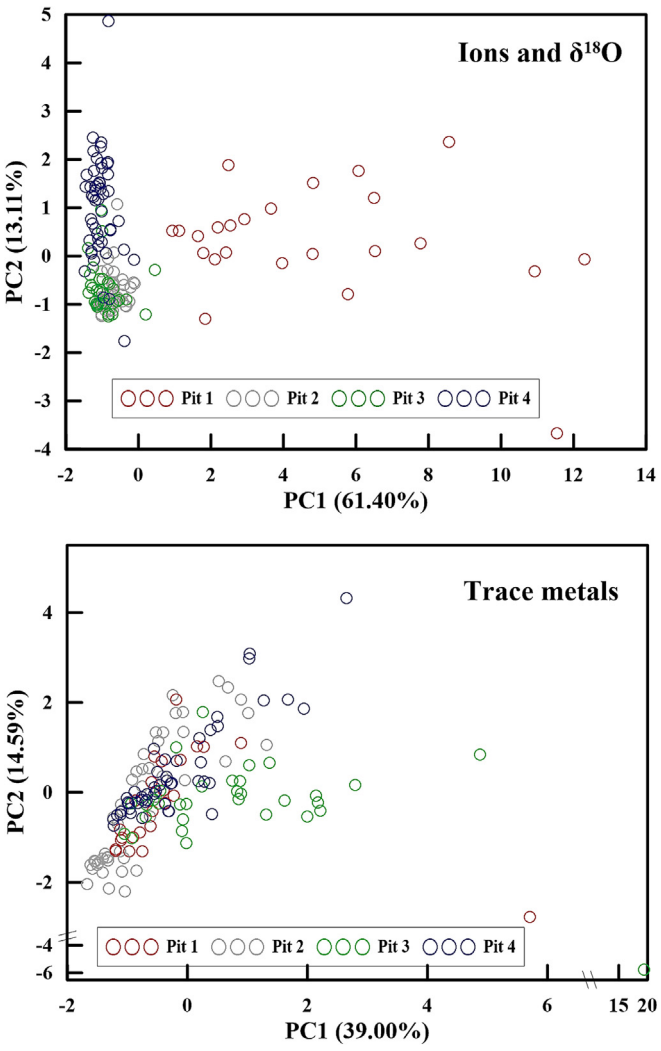


Fig. 4. PCA plots (PC1 vs PC2) for the four snow pits. Total variances are indicated on each axis.

The monthly mean concentrations of the trace elements for the period 1999–2002 were estimated (but not shown). In Pit 2, positive correlations among these concentrations suggest seasonally consistent transport patterns from potential sources. This assumption also applies to Pit 3, where positive correlations are observed among the concentrations of most elements, except for U and As. Conversely, Pits 1 and 4 appear to have multiple sources with distinct transport patterns. The seasonal mean concentrations of the trace elements are summarized in Supplementary Data Table S3. In Pit 1, the concentrations of most elements (except for U, Bi, and As) are elevated during the austral spring (SON), whereas in Pit 3, high elemental concentrations (except for Mn and Fe) are observed during the austral winter (JJA). Pit 2 also displays elevated concentrations during JJA, SON, and the austral summer (DJF), while Pit 4 records high elemental concentrations during DJF. These patterns indicate that the concentrations of the trace elements in Pits 2 and 3 likely increased during the austral winter, suggesting similar atmospheric transport mechanisms. This is consistent with the windy conditions typically experienced in this region during the winter (Allison, 1998; Tang et al., 2020; Ding et al., 2022). However, establishing consistent seasonal variation trends in trace element concentrations is challenging due to occasional peaks occurring in different seasons (Hur et al., 2007). These peaks can be sensitive to various factors, including precipitation type and post-depositional effects (Tuohy et al., 2015; Nyamgerel et al., 2024). Post-depositional effects, such as snow redistribution, wind-driven blowing, and ablation, are substantial (Ding et al., 2011) and can affect trace element concentrations (Tuohy et al., 2015). In particular, the redistribution and removal of snow layers during strong storm events can significantly alter (or smooth) the

Table 2
Correlation matrix of the trace elements found in the snow pits. Higher (r > 0.4) values are highlighted in bold and underlined.

	Cd	Ba	Pb	U	Bi	V	Mn	Fe	Cu	Zn	As
Pit 1											
Cd	1.00										
Ba	0.39	1.00									
Pb	0.36	**0.98**	1.00								
U	−0.09	−0.10	−0.24	1.00							
Bi	0.13	−0.06	−0.10	0.09	1.00						
V	0.21	0.27	0.13	**0.40**	0.34	1.00					
Mn	**0.42**	**0.63**	**0.57**	0.08	0.19	**0.61**	1.00				
Fe	0.33	**0.61**	**0.57**	−0.01	0.18	**0.50**	**0.68**	1.00			
Cu	0.22	0.13	0.11	0.27	0.05	0.30	0.15	0.18	1.00		
Zn	**0.45**	**0.95**	**0.97**	−0.32	−0.15	0.12	**0.51**	**0.50**	0.04	1.00	
As	0.14	−0.11	−0.20	**0.72**	0.31	0.30	−0.05	0.13	0.33	−0.28	1.00
Pit 2											
Cd	1.00										
Ba	**0.54**	1.00									
Pb	**0.60**	**0.72**	1.00								
U	**0.55**	**0.63**	**0.72**	1.00							
Bi	**0.64**	**0.57**	**0.73**	**0.78**	1.00						
V	0.15	**0.40**	0.16	0.00	0.04	1.00					
Mn	**0.55**	**0.80**	**0.72**	**0.70**	**0.75**	0.36	1.00				
Fe	**0.41**	**0.70**	**0.61**	**0.50**	**0.61**	0.31	**0.78**	1.00			
Cu	0.07	0.21	0.37	**0.49**	0.37	−0.05	0.31	**0.41**	1.00		
Zn	0.34	**0.63**	**0.54**	0.23	0.14	0.39	0.35	0.25	0.07	1.00	
As	**0.52**	0.34	**0.49**	**0.54**	**0.81**	0.14	**0.53**	0.39	0.20	−0.03	1.00
Pit 3											
Cd	1.00										
Ba	**0.67**	1.00									
Pb	**0.45**	**0.89**	1.00								
U	0.22	**0.38**	0.30	1.00							
Bi	**0.63**	**0.55**	**0.47**	**0.47**	1.00						
V	0.20	**0.61**	**0.57**	**0.70**	**0.41**	1.00					
Mn	0.29	**0.84**	**0.81**	0.23	0.29	**0.58**	1.00				
Fe	0.25	**0.82**	**0.81**	0.22	0.27	**0.58**	**0.99**	1.00			
Cu	**0.77**	**0.66**	**0.50**	0.16	0.37	0.36	**0.47**	**0.45**	1.00		
Zn	**0.79**	**0.90**	**0.85**	0.29	**0.55**	**0.48**	**0.65**	**0.63**	**0.77**	1.00	
As	**0.51**	0.27	0.15	0.03	**0.65**	−0.01	0.08	0.07	0.29	0.29	1.00
Pit 4											
Cd	1.00										
Ba	0.19	1.00									
Pb	0.33	**0.59**	1.00								
U	0.19	**0.74**	**0.55**	1.00							
Bi	0.18	**0.49**	**0.70**	**0.52**	1.00						
V	0.19	**0.75**	**0.61**	**0.74**	**0.58**	1.00					
Mn	0.15	**0.76**	**0.60**	**0.73**	**0.57**	**0.94**	1.00				
Fe	−0.02	**0.41**	0.27	**0.42**	0.22	**0.55**	**0.53**	1.00			
Cu	0.26	**0.43**	**0.41**	0.20	0.28	0.30	0.32	0.30	1.00		
Zn	0.14	0.10	0.11	−0.16	−0.06	−0.14	−0.12	−0.11	**0.55**	1.00	
As	0.40	**0.43**	**0.68**	**0.51**	**0.71**	**0.57**	**0.52**	0.29	0.24	−0.13	1.00

original trace element concentrations (Fortner et al., 2011; Tuohy et al., 2015). In the study area, winter snow layers are particularly susceptible to these wind-driven effects (Ding et al., 2022), and the accumulation rate may also be relatively high during this period (Tuohy et al., 2015). However, as mentioned above, this assumption is not straightforward for all snow pits, indicating disparities during the release, transport, deposition, and accumulation of trace elements.

The PCA results for isotopes, ions, and trace elements in each snowpit are summarized in Supplementary Data Table S4–S7. Pits 2 and 3 exhibit similar variable clustering patterns in the principal components (PCs), whereas Pits 1 and 4 display distinct patterns. In Pit 1, all ions (except MSA) cluster in PC1 alongside U, As, V, and Zn. Meanwhile, most other elements are classified in PC 2, indicating the dominant influence of oceanic air masses. Conversely, in Pits 2 and 3, $\delta^{18}O$, ions (except for MSA and $nssSO_4^{2-}$), and most trace elements cluster in PC1, suggesting similar air mass sources in these locations. In Pit 4, an inland site, trace elements and some ions (except MSA, $nssSO_4^{2-}$, and NO_3^-) cluster in PC1, indicating potential differences in sources at this site. Overall, according to these PCA results, oceanic sources dominate in Pit 1, while other sources, such as continental influences, affect Pits 2, 3, and

Table 3
Sample counts expressed as a percentage of the total number (n) of samples of each element, categorized by the range of the crustal enrichment factor (EF_c) in the snow pit samples during the period 1999–2002. Larger values are highlighted in bold.

Pit 1											
EF_c	Cd	Ba	Pb	U	Bi	V	Mn	Fe	Cu	Zn	As
<10	0	**96**	0	13	0	**100**	**96**	**100**	0	4	0
10–100	0	4	**96**	**88**	4	0	4	0	46	**88**	0
100–1000	**92**	0	0	0	**96**	0	0	0	**54**	4	**67**
>1000	8	0	4	0	0	0	0	0	0	4	33
Pit 2											
EF_c	Cd	Ba	Pb	U	Bi	V	Mn	Fe	Cu	Zn	As
<10	14	**100**	0	**86**	0	**96**	**100**	**100**	0	0	4
10–100	0	0	**50**	14	0	4	0	0	11	46	0
100–1000	**50**	0	**50**	0	**50**	0	0	0	**86**	54	11
>1000	36	0	0	0	**50**	0	0	0	4	0	**86**
Pit 3											
EF_c	Cd	Ba	Pb	U	Bi	V	Mn	Fe	Cu	Zn	As
<10	0	**100**	4	**60**	0	**100**	**84**	**84**	0	0	0
10–100	0	0	**60**	40	4	0	16	12	12	0	0
100–1000	44	0	36	0	44	0	0	4	**84**	32	20
>1000	56	0	0	0	**52**	0	0	0	4	**68**	**80**
Pit 4											
EF_c	Cd	Ba	Pb	U	Bi	V	Mn	Fe	Cu	Zn	As
<10	0	**100**	4	**90**	0	**100**	**100**	**95**	0	0	0
10–100	0	0	**88**	10	0	0	0	5	**69**	**58**	0
100–1000	**92**	0	8	0	**92**	0	0	0	31	42	**64**
>1000	8	0	0	0	8	0	0	0	0	0	36

Table 4
Sample counts expressed as a percentage of the total number (n) of samples of each element, categorized by the range of the marine enrichment factor (EF_m) in the snow pit samples during the period 1999–2002. Larger values are highlighted in bold.

Pit 1											
EF_m	Cd	Ba	Pb	U	Bi	V	Mn	Fe	Cu	Zn	As
<10	0	**92**	0	**100**	25	**83**	0	0	0	25	0
10–100	**88**	8	0	0	**75**	17	0	0	0	**67**	**96**
100–1000	13	0	25	0	0	0	**83**	38	**79**	8	4
>1000	0	0	75	0	0	0	17	**63**	21	0	0
Pit 2											
EF_m	Cd	Ba	Pb	U	Bi	V	Mn	Fe	Cu	Zn	As
<10	14	0	0	**93**	0	0	0	0	0	0	4
10–100	0	**79**	0	7	0	**79**	0	0	0	0	0
100–1000	**68**	21	0	0	**82**	21	4	0	0	**71**	**75**
>1000	18	0	**100**	0	18	0	**96**	**100**	**100**	29	21
Pit 3											
EF_m	Cd	Ba	Pb	U	Bi	V	Mn	Fe	Cu	Zn	As
<10	0	0	0	**88**	0	0	0	0	0	0	0
10–100	0	**52**	0	12	0	**72**	0	0	0	0	0
100–1000	**60**	44	0	0	**72**	28	0	0	0	0	**64**
>1000	40	4	**100**	0	28	0	**100**	**100**	**100**	**100**	36
Pit 4											
EF_m	Cd	Ba	Pb	U	Bi	V	Mn	Fe	Cu	Zn	As
<10	0	0	0	**54**	0	0	0	0	0	0	0
10–100	0	38	0	46	0	46	0	0	0	0	0
100–1000	46	**62**	0	0	**62**	**54**	0	0	0	23	46
>1000	**54**	0	**100**	0	38	0	**100**	**100**	**100**	**77**	**54**

4. By separating the trace elements from isotopes and ions, the PCA plot effectively illustrates the differences among snow pits, particularly highlighting the distinctions between Pits 1 and 4 (Fig. 4).

According to the correlation analysis of the trace elements, the concentration of Ba, a representative crustal-sourced element, correlates with the concentrations of most metals in Pits 2, 3, and 4 (Table 2). This suggests similarities in the sources, transport mechanisms, and depositional patterns of trace elements across these inland snow pits. In contrast, Pit 1 exhibits distinct correlation trends, indicating the dominant influence of oceanic air masses (Table 2). Notably, several elements in Pits 1 (U, Bi, V, Cu, and As), 2 (V, Cu, Zn, and As), 3 (U, Bi, and As), and 4 (Cd, Cu, Zn, and As) show no clear correlations, suggesting the presence of various sources for these elements.

3.2. Source identification of trace elements

3.2.1. Crustal and marine enrichment

The topography of the Lambert Glacier Basin plays a crucial role in controlling the katabatic wind regime and surface climatic conditions (Allison, 1998). Poleward-moving air masses are believed to dominate the eastern side of the Lambert Glacier Basin (Xiao et al., 2004), which is characterized by relatively steep slopes and strong winds (>10 m s^{-1}) based on observations from 1982 to 1996 (Allison, 1998). Air mass trajectories for the inland Dome A site from 1950 to 2016 identify the South Atlantic and South Indian Ocean sectors as the dominant sources of these air masses (Liu et al., 2021). During winter, trajectory data from 2012 to 2016 indicate the dominance of slower-moving oceanic air masses (Liu et al.,

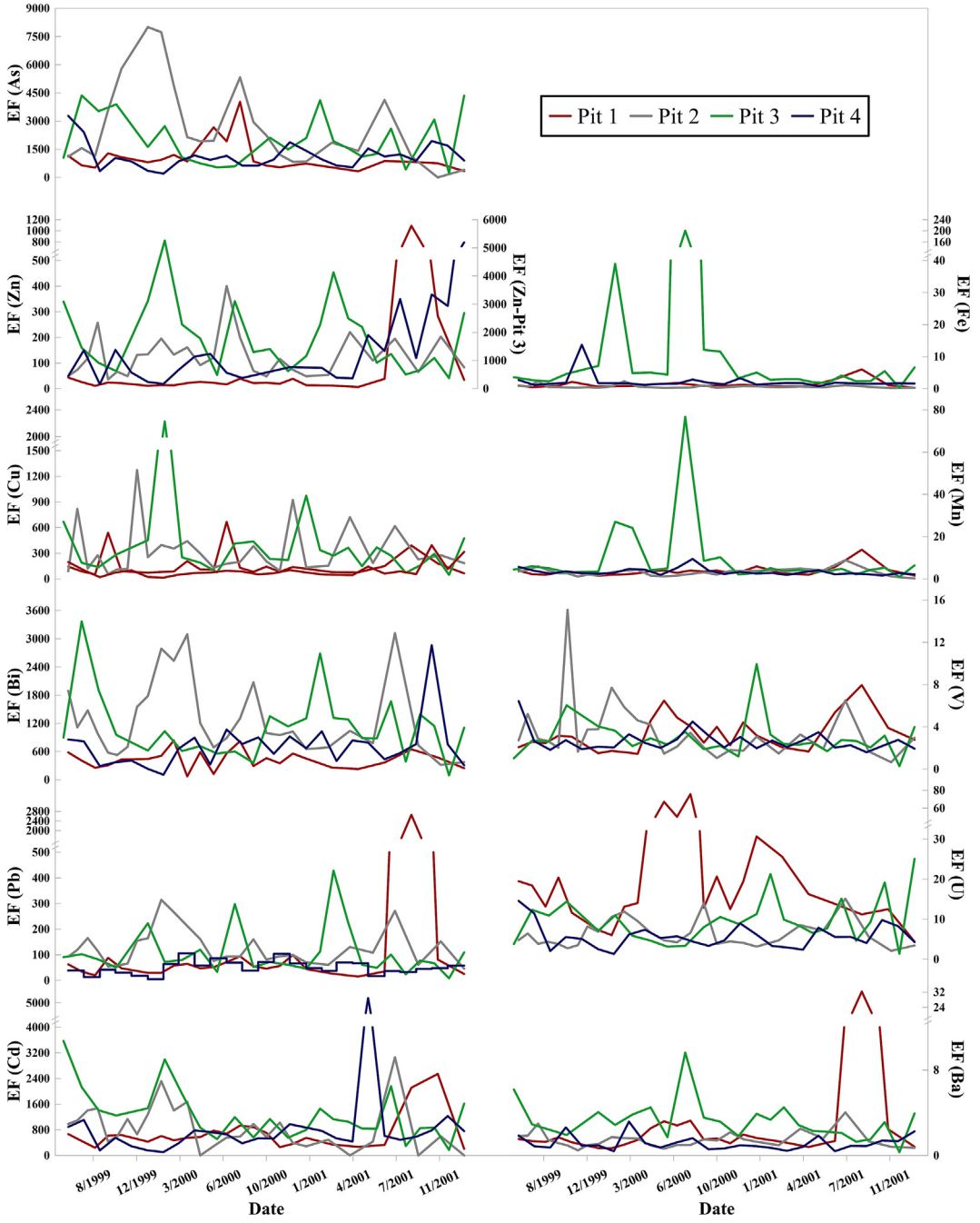


Fig. 5. Temporal variations in the crustal enrichment factors (EF_c) of the snow pits during the period 1999–2002.

2019). Meanwhile, faster-moving air mass trajectories are observed during summer, covering a broad coastal area of East Antarctica (Liu et al., 2019). To identify the potential sources of trace elements, analyses were conducted on the selected snow pits from 1999 to 2002. In this analysis, trace elements were categorized based on their crustal (EF_c) and marine (EF_m) enrichment factors. Tables 3 and 4 provide details of these factors for all metals.

Temporal variations in the EF_c values of non-crustal elements (Cd, Bi, Zn, Pb, Cu, and As) and crustal elements (Ba, U, V, Mn, and Fe) are illustrated in Fig. 5. Each snowpit exhibits distinct temporal trends for these metals, with no clear correlation to distance from the coast. A predominant contribution from crustal sources is evident for Ba, U (except in Pit 1), V, Mn, and Fe across all snowpits, as indicated by their low EF_c values ($EF_c < 10$). Additionally, the crustal contribution of U is significant in Pits 2, 3, and 4 (inland sites), whereas Pit 1 shows slightly elevated EF_c values, suggesting mixed contributions from multiple sources at this site (Fig. 5).

Notably, the EF_c values for Cd, Pb, Bi, Cu, Zn, and As exceed 10, indicating significant non-crustal contributions to these elements in all snowpits. Pits 2 and 3, in particular, exhibit relatively higher EF_c values, suggesting a dominant influence of non-crustal sources at these sites. A highly enriched As ($EF_c > 1000$) is observed across all snowpits, while similarly elevated EF_c values for Cd and Bi ($EF_c > 1000$) are detected in Pits 2 and 3 (Fig. 5). Additionally, the EF_c values for Zn in Pits 3 and 4 are substantially higher than those in Pits 1 and 2.

Local ice-free areas near the Lambert Glacier Basin significantly influence the distribution of trace elements in the selected snow pits. Mineralogical studies have shown high concentrations of Pb, Th, and U in nearby locations, such as the Larsemann Hills (Gasparon and Matschullat, 2006), where anthropogenic pollution in the topsoils is minimal (Shi et al., 2018). To distinguish the contribution of local crustal sources, enrichment factor (EF_c) values were calculated for Pb, Mn, Fe, Cu, and Zn using the local mineral composition in the Larsemann Hills (Shi et al., 2018). Crustal contributions were dominant for most samples (>84.00% of the total count) of Mn and Fe, which had low EF_c values ($EF_c < 10$), whereas non-crustal sources were dominant for Pb, Cu, and Zn (>92.31% of the total count), which had high EF_c values ($EF_c > 10$). This suggests mixed contributions from both local and remote crustal sources (Du et al., 2018; Herath et al., 2024), along with distinct transport and deposition characteristics at each snow pit location. Previous studies have reported anthropogenic contributions to the concentrations of Pb, As, Cd, and Cu (Hur et al., 2007; Jiang et al., 2018; Xu et al., 2020; Liu et al., 2021), which is consistent with the results of the present study. Notably, the primary anthropogenic contributions in the study region originate from activities in Australia, South America, and South Africa (Planchon et al., 2002; Du et al., 2018; Herath et al., 2024), as well as from local Antarctic research stations (Herath et al., 2024). The substantial and inconsistent variations observed in EF_c values can be attributed to the complex characteristics of the source, transport pathway, and deposition pattern in the study region, as similarly reported for Pb, As, and Cu (Jiang et al., 2018). These characteristics may include the mixing of air masses (marine and continental), post-depositional effects (such as snow redistribution and wind-driven blowing), and deposition types (wet and dry deposition) (Ding et al., 2011; Jiang et al., 2018).

In Pit 1, the EF_c values of U, Bi, Cu, and As show no correlations with those of other elements. Similarly, in Pit 2, no correlations are observed among the EF_c values of V, Cu, and Zn. In Pit 3, several elements, including Cd, Pb, U, Bi, V, Cu, and As, exhibit distinct temporal variations. In Pit 4, no correlations are observed among the EF_c values of most trace elements. These observations suggest that the snowpits experience distinct temporal variations, mixed contributions from various sources, and complex atmospheric circulation patterns. Meanwhile, the EF_c values of trace elements indicate that Ba, U, and V in Pit 1 originate from marine sources ($EF_c < 10$) (Table 4). Across Pits 2, 3, and 4, U consistently exhibits low EF_c values ($EF_c < 10$), which is consistent with previous research indicating that U predominantly originates from sea-salt aerosols in Antarctic snow and ice (Henderson et al., 2006). The distribution

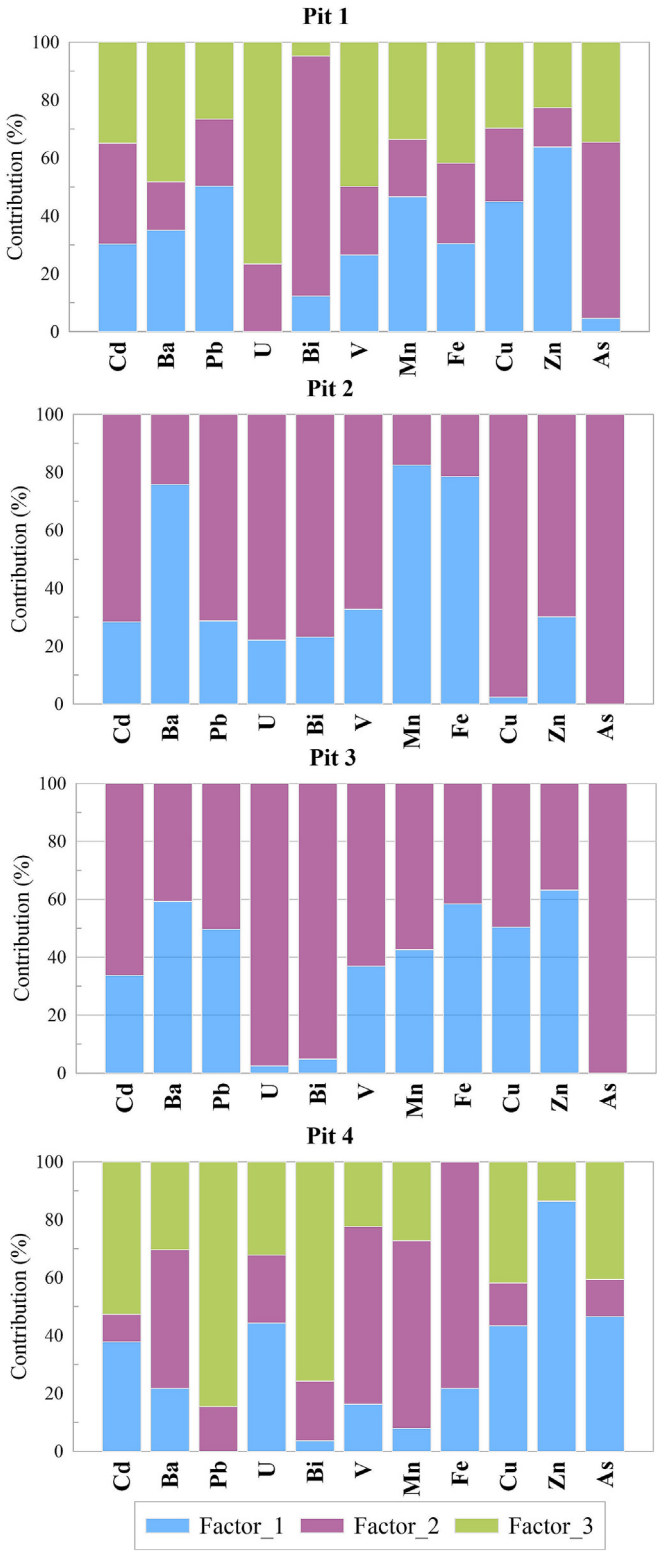


Fig. 6. Percentage contributions of each metal in the factor profiles derived from the PMF analysis of the trace elements in the snow pits from 1999 to 2002.

of trace elements in coastal oceans is dynamic and complex (Bruland and Lohan, 2003). Both sea salt (oceanic sources) and local dust from ice-free areas contribute substantially to trace element concentrations in regions within 0–100 km of the coast (Du et al., 2019). Overall, the coastal region of the study site is considered to be influenced by mixed sources, including cyclonic activities (marine) along the coast and katabatic winds (continental) (Jiang et al., 2018). Inland sites, on the other hand, are likely influenced by air masses carrying mineral dust and anthropogenic pollutants from low-latitude areas (e.g., Australia and South Africa) (Du et al., 2019). These observations are consistent with the findings of the present study, which examined snow pits.

Table 5
Percentage contributions (%) of each metal in the factor profiles derived from the PMF analysis of the four snow pits.

	Pit 1			Pit 2		Pit 3		Pit 4		
	Factor 1	Factor 2	Factor 3	Factor 1	Factor 2	Factor 1	Factor 2	Factor 1	Factor 2	Factor 3
Cd	30.30	34.81	34.88	28.38	71.62	33.75	66.25	37.82	9.50	52.68
Ba	35.07	16.69	48.25	75.81	24.19	59.28	40.72	21.75	47.90	30.35
Pb	50.30	23.15	26.54	28.75	71.25	49.68	50.32	0.00	15.46	84.54
U	0.00	23.44	76.56	22.08	77.92	2.51	97.49	44.33	23.46	32.21
Bi	12.30	82.93	4.77	23.15	76.85	4.81	95.19	3.67	20.62	75.71
V	26.52	23.63	49.85	32.76	67.24	36.91	63.09	16.31	61.35	22.34
Mn	46.64	19.77	33.60	82.48	17.52	42.60	57.40	7.96	64.83	27.21
Fe	30.43	27.81	41.76	78.56	21.44	58.43	41.57	21.75	78.25	0.00
Cu	44.94	25.37	29.69	2.40	97.60	50.38	49.62	43.33	14.85	41.81
Zn	63.80	13.56	22.64	30.15	69.85	63.18	36.82	86.30	0.17	13.53
As	4.62	60.87	34.52	0.00	100.00	0.00	100.00	46.56	12.82	40.62

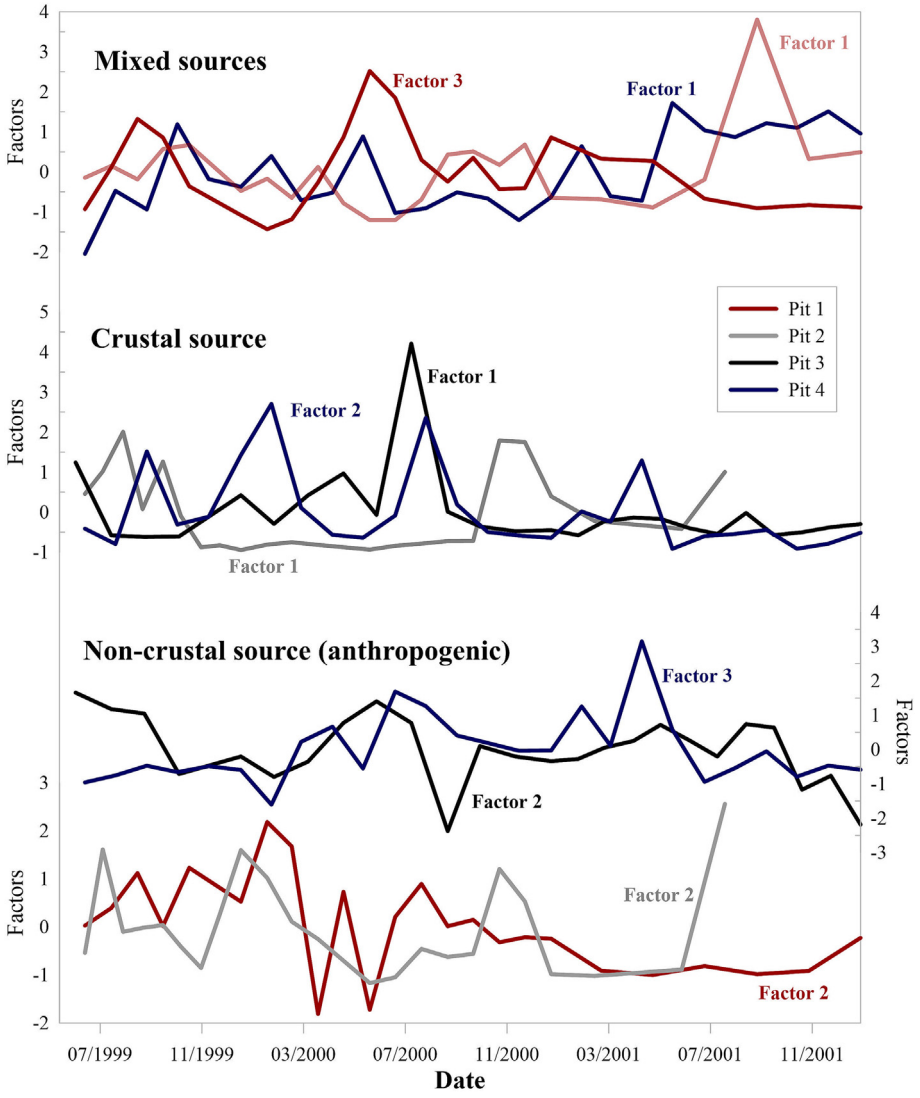


Fig. 7. Comparison of the temporal variation trends of the PMF factors (standardized) for the snow pits.

3.2.2. Source contributions

To quantify the source contributions detailed in Section 3.2.1, positive matrix factorization (PMF) analysis was performed on the trace element concentrations observed between 1999 and 2002. Fig. 6 and Table 5 show the percentage contributions of each metal in the snow pits, categorized by the identified sources.

In Pit 2, Factor 1 shows high percentages for Ba (75.81%), Mn (82.48%), and Fe (78.56%), indicating that these elements originate from mineral dust. In contrast, Factor 2 exhibits high percentages for Cd (71.62%), Pb (71.25%), U (77.92%), Bi (76.85%), Cu (97.60%), and As (100.00%), suggesting non-crustal origins, likely anthropogenic. Similarly, in Pit 3, Factor 1 shows high percentages for Ba (59.28%), Fe (59.43%), and zinc (Zn) (63.18%), whereas Factor 2 exhibits high percentages for U (97.49%), Bi (95.19%), and As (100.00%). Overall, the factors mentioned above indicate relatively consistent and dominant contributions of these sources to the trace element concentrations in Pits 2 and 3.

In Pit 4, Factor 1 shows high contributions of Cd (37.8%), U (44.33%), Cu (43.33%), Zn (86.30%), and As (46.56%), indicating a non-crustal source, likely a mix of anthropogenic and sea-salt influences. Factor 3 clusters Cd (52.68%), Cu (41.81%), and As (40.62%) with Pb (84.54%) and Bi (75.71%), further confirming a non-crustal origin, most likely anthropogenic. In contrast, Factor 2 exhibits high contributions of Ba (47.90%), V (61.35%), Mn (64.83%), and Fe (78.25%), suggesting a mineral dust source.

In Pit 1, Factor 1 exhibits high percentages of Pb (50.30%), Mn (46.64%), Cu (44.94%), and Zn (63.80%). Meanwhile, Factor 2 is dominated by Bi (82.93%) and As (60.87%), suggesting a potential anthropogenic source. Factor 3 displays high percentages of Ba (48.25%), U (76.56%), V (49.85%), and Fe (41.76%). Given the EF_m values of Ba, U, and V (Table 4), Factor 3 likely indicates an oceanic source. However, it is unlikely that these elements in Pit 1 originate from a single source; instead, they are plausibly derived from a mix of crustal and oceanic sources. Compared to the other snowpits, identifying sources through PMF analysis in Pit 1 was more challenging, likely due to mixed contributions and the influence of highly variable cyclonic activity in the ocean (Du et al., 2019; Xu et al., 2019).

Fig. 7 illustrates the temporal variations of the factors identified through the PMF analysis. Although these temporal variations differ among the snow pits, some similarities are observed in the factors representing non-crustal sources in Pits 1 and 2. Moreover, the factors representing non-crustal sources in Pits 3 and 4 show consistent peaks, with both pits also sharing similarities in the factors associated with crustal sources, indicating similarities in emission sources and atmospheric transport patterns. Variations in other factors indicating mixed sources in Pits 1 (Factors 1 and 3) and 4 (Factor 1) probably reflect similarities in atmospheric transport characteristics.

Therefore, our previous source identification based on PCA was further refined by PMF analysis. This facilitated more detailed source apportionment and provided quantitative estimates of source contributions, leading to a better understanding of trace element sources. The combined use of these methods provides clearer insights (e.g., Chavent et al., 2009), as the factors derived from the PMF analysis allow for comprehensive interpretations of trace element distributions in ice cores. Such distributions are often difficult to examine due to their sporadic and highly variable nature.

4. Conclusions

This study investigated the spatial distributions and sources of various trace elements, including Cd, Ba, Pb, U, Bi, V, Mn, Fe, Cu, Zn, and As, within four snowpits located in the Lambert Glacier Basin, East Antarctica. These snowpits were positioned at different elevations and distances from the coast. The trace element concentrations exhibited site-, element-, and season-dependent variations, with notably higher concentrations observed at the inland sites (Pits 3 and 4). Unlike $\delta^{18}O$ and ion concentrations, which decreased with increasing distance from the coast and elevation, trace element concentrations highlighted the significance of emission intensity from a single dominant source (marine). The results suggest that elements such as Ba, U, V, Mn, and Fe primarily originate from crustal sources, while Cd, Bi, Zn, Pb, Cu, and As are derived from non-crustal sources. PMF analysis further clarified source contributions, revealing that elemental concentrations in Pits 2 and 3 were influenced by both crustal sources (Ba, Mn, Fe, and Zn) and non-crustal, possibly anthropogenic sources (Cd, Pb, U, Bi, Cu, and As). Similarly, elemental concentrations in Pit 4 (an inland site) reflected mixed contributions from both crustal and non-crustal sources. Meanwhile, Pit 1 (a coastal site) exhibited mixed-source influences, shaped by a highly dynamic marine climate and environment. Temporal variations in the factors derived from PMF analysis indicated similarities in emission sources and atmospheric transport patterns among certain snowpits, providing a foundation for more comprehensive interpretations of trace element distributions in longer ice core records. Overall, the findings of this study offer valuable insights into the atmospheric distribution of trace elements and are expected to contribute to paleoclimate studies based on extended ice core records.

CRediT authorship contribution statement

Yalalt Nyamgerel: Conceptualization, Formal analysis, Writing – original draft, Writing –review and editing. **Soon Do Hur:** Funding acquisition, Formal analysis, Writing – review and editing. **Tseren-Ochir Soyol-Erdene:** Writing – review and editing. **Xiao Cunde:** Writing – review and editing. **Hyejung Jung:** Writing – review and editing. **Jeonghoon Lee:** Conceptualization, Writing – review and editing.

Declaration of competing interest

The authors declare that they have no known competing financial interests or personal relationships that could have appeared to influence the work reported in this paper.

Acknowledgements

This research was supported by the Korea Polar Research Institute grant (PE25100) and the National Research Foundation of Korea grant funded by the Korean Government (NRF2022R1A2C3007047). This study was partially supported by Korea Institute of Marine Science & Technology Promotion (KIMST) and by the Ministry of Oceans and Fisheries (RS-2023-00256677; PM23020).

Appendix A. Supplementary data

Supplementary data to this article can be found online at https://doi.org/10.1016/j.gsf.2025.102045.

References

Allison, I., 1998. Surface climate of the interior of the Lambert Glacier basin, Antarctica, from automatic weather station data. Ann. Glaciol. 27, 515–520. https://doi.org/10.3189/1998AoG27-1-515-520.

Barbante, C., Turetta, C., Gambaro, A., Capodaglio, G., Scarponi, G., 1998. Sources and origins of aerosols reaching Antarctica as revealed by lead concentration profiles in shallow snow. Ann. Glaciol. 27, 674–678. https://doi.org/10.3189/1998AoG27-1-674-678.

Bruland, K.W., Lohan, M.C., 2003. 6.02 – Controls of trace metals in seawater. Treatise on Geochemistry 6, 23–47. https://doi.org/10.1016/B0-08-043751-6/06105-3.

Cesari, D., Amato, F., Pandolfi, M., Alastuey, A., Querol, X., Contini, D., 2016. An inter-comparison of PM_{10} source apportionment using PCA and PMF receptor models in three European sites. Environ. Sci. Pollut. Res. 23, 15133–15148. https://doi.org/10.1007/s11356-016-6599-z.

Chavent, M., Guégan, H., Kuentz, V., Patouille, B., Saracco, J., 2009. PCA- and PMF-based methodology for air pollution sources identification and apportionment. Environmetrics 20, 928–942. https://doi.org/10.1002/env.963.

Dixon, D.A., Mayewski, P.A., Korotkikh, E., Sneed, S.B., Handley, M.J., Introne, D.S., Scambos, T.A., 2013. Variations in snow and firn chemistry along US ITASE traverses and the effect of surface glazing. The Cryosphere 7 (2), 515–535. https://doi.org/10.5194/tc-7-515-2013.

Du, Z., Xiao, C., Ding, M., Li, C., 2018. Identification of multiple natural and anthropogenic sources of dust in snow from Zhongshan Station to Dome A, East Antarctica. J. Glaciol. 64 (248), 855–865. https://doi.org/10.1017/jog.2018.72.

Du, Z., Xiao, C., Handley, M.J., Mayewski, P.A., Li, C., Liu, S., Ma, X., Yang, J., 2019. Fe variation characteristics and sources in snow samples along a traverse from Zhongshan Station to Dome A, East Antarctica. Sci. Total Environ. 675, 380–389.

Du, Z., Xiao, C., Mayewski, P., Handley, M.J., Li, C., Ding, M., Liu, J., Yang, J., Liu, K., 2020. The iron records and its sources during 1990–2017 from the Lambert Glacial Basin shallow ice core, East Antarctica. Chemosphere 251, 126399.

Ding, M., Xiao, C., Li, Y., Ren, J., Hou, S., Jin, B., Sun, B., 2011. Spatial variability of surface mass balance along a traverse route from Zhongshan station to Dome A, Antarctica. J. Glaciol. 57 (204), 658–666. https://doi.org/10.3189/002214311797409820.

Ding, M., Zou, X., Sun, Q., Yang, D., Zhang, W., Bian, L., Lu, C., Allison, I., Heil, P., Xiao, C., 2022. The PANDA automatic weather station network between the coast and Dome A, East Antarctica. Earth Syst. Sci. Data 14, 5019–5035. https://doi.org/10.5194/essd-14-5019-2022.

Fischer, B.M.C., Meerveld, H.J., Seibert, J., 2017. Spatial variability in the isotopic composition of rainfall in a small headwater catchment and its effect on hydrograph separation. J. Hydrol. 547, 755–769. https://doi.org/10.1016/j.jhydrol.2017.01.045.

Fortner, S.K., Lyons, W.B., Olesik, J.W., 2011. Eolian deposition of trace elements onto Taylor Valley Antarctic glaciers. Appl. Geochem. 26–11, 1897–1904. https://doi.org/10.1016/j.apgeochem.2011.06.013.

Fricker, H.A., Allison, I., Craven, M., Hyland, G., Ruddell, A., Young, N., Coleman, R., Kind, M., Krebs, K., Popov, S., 2002. Redefinition of the grounding zone of the Amery Ice Shelf, East Antarctica, grounding zone. J. Geophys. Res. 107 (B5), ECV 1–1-ECV 1–9. doi:10.1029/2001JB000383.

Gabrielli, P., Planchon, F., Barbante, C., Boutron, C.F., Petit, J.R., Bulat, S., Hong, S., Gozzi, G., Cescon, P., 2009. Ultra-low rare earth element content in accreted ice from sub-glacial Lake Vostok, Antarctica. Geochim. Cosmochim. Acta 73 (20), 5959–5974. https://doi.org/10.1016/j.gca.2009.05.050.

Gabrielli, P., Wegner, A., Petit, J.R., Delmonte, B., De Deckker, P., Gaspari, V., Fischer, H., Ruth, U., Kriews, M., Boutron, C., Cescon, P., Barbante, C., 2010. A major glacial-interglacial change in aeolian dust composition inferred from Rare Earth Elements in Antarctic ice. Quat. Sci. Rev. 29 (1–2), 265–273. https://doi.org/10.1016/j.quascirev.2009.09.002.

Gasparon, M., Matschullat, J., 2006. Trace metals in Antarctic ecosystems: results from the Larsemann Hills, East Antarctica. Appl. Geochem. 21 (9), 1593–1612.

Görlach, U., Boutron, C.F., 1990. Preconcentration of lead, cadmium, copper and zinc in water at the pg g^{-1} level by nonboiling evaporation. Anal. Chim. Acta 236, 391–398.

Han, C., Hwang, H., Kang, J.H., Hong, S.B., Han, Y., Lee, K., Hur, S.D., Hong, S., 2020. Reliable ultra trace analysis of Cd, U and Zn concentrations in Greenland snow and ice by using ultraclean methods for contamination control. Molecules 25 (11), 2519. https://doi.org/10.3390/molecules25112519.

Henderson, G.M., Hall, B.L., Smith, A., Robinson, L.F., 2006. Control on ($^{234}U/^{238}U$) in lake water: a study in the Dry Valleys of Antarctica. Chem. Geol. 226 (3–4), 298–308. https://doi.org/10.1016/j.chemgeo.2005.09.026.

Herath, I.K., Ma, H., Bargagli, R., Hu, Y., Hirabayashi, M., Motoyama, H., Shi, G., 2024. Sources and distribution of trace elements in surface snow from coastal Zhongshan Station to Dome A (East Antarctica). Atmos. Environ. 331, 120583.

Hong, S., Lluberas, A., Rodriguez, F., 2000a. A clean protocol for determining ultralow heavy metal concentrations: its application to the analysis of Pb, Cd, Cu, Zn and Mn in Antarctic snow. Korean J. Polar Res. 11, 35–47.

Hong, S., Lee, G., Van de Velde, K., Boutron, C.F., 2000b. Variability of Pb, Mn, Al and Na concentrations in snow deposited from winter and early summer 1998 in Livingston Island, Antarctic Peninsula. Journal of Korean Society for. Atmos. Environ. 16 (E-2), 85–96.

Hong, S., Soyol-Erdene, T.O., Hwang, H.J., Hong, S.B., Hur, S.D., Motoyama, H., 2012. Evidence of global-scale as, Mo, Sb, and Tl atmospheric pollution in the Antarctic snow. Environ. Sci. Technol. 46 (21), 11550–11557. https://doi.org/10.1021/es303086c.

Hong, S., Han, C.H., Hwang, H.J., Soyol-Erdene, T.-O., Kang, J.H., Hur, S.D., Burn-Nunes, L.J., Gabrielli, P., Barbante, C., Boutron, C.F., 2013. Trace elements and Pb isotope record in Dome C (East Antarctica) ice over the past 800,000 years. E3S Web Conf. 1, 23001. https://doi.org/10.1051/e3sconf/20130123001.

Huang, W., Yan, M., Mulvaney, R., Qian, Z., Liu, L., An, C., Xiao, C., Zhang, Y., 2021. Spatial variability of glaciochemistry along a transect from Zhongshan Station to LGB69, Antarctica. Atmosphere 12, 393. https://doi.org/10.3390/atmos12030393.

Hur, S.D., Ming, Y., Barbante, C., Boutron, C.F., Lee, K., Gabrielli, P., Hong, S.-H., Xiao, C., 2007. Seasonal patterns of heavy metal deposition to the snow on Lambert Glacier basin, East Antarctica. Atmos. Environ. 41, 8567–8578. https://doi.org/10.1016/j.atmosenv.2007.07.012.

Ito, K., Xue, N., Thurston, G., 2004. Spatial variation of PM2.5 chemical species and source-apportioned mass concentrations in New York City. Atmos. Environ. 38, 5269–5282.

Jiang, X.X., Hou, S., Li, Y.S., Pang, H.X., Hua, R., Paul, M., Sharon, S., An, C.L., Michael, H., Liu, K., Zhang, W.B., 2018. Spatial variations of Pb, As, and Cu in surface snow along the transect from the Zhongshan Station to Dome A, East Antarctica. Sciences in Cold and Arid Regions 10 (3), 219–231. https://doi.org/10.3724/SP.J.1226.2018.00219.

Kakareka, S., Kukharchyk, T., Kurman, P., 2020. Study of trace elements in the surface snow for impact monitoring in Vecherny Oasis, East Antarctica. Environ. Monit. Assess 192, 725. https://doi.org/10.1007/s10661-020-08682-8.

Lee, K.S., Grundstein, A.J., Wenner, D.B., Choi, M.S., Woo, N.C., Lee, D.H., 2003. Climatic controls on the stable isotopic composition of precipitation in Northeast Asia. Clim. Res. 23, 137–148. https://doi.org/10.3354/cr023137.

Li, C., Kang, S., Shi, G., Huang, J., Ding, M., Zhang, Q., Zhang, L., Guo, J., Xiao, C., Hou, S., Sun, B., Qin, D., Ren, J., 2014. Spatial and temporal variations of total mercury in Antarctic snow along the transect from Zhongshan Station to Dome A. Tellus b: Chemical and Physical Meteorology 66 (1), 25152. https://doi.org/10.3402/tellusb:v66.25152.

Li, C., Xiao, C., Shi, G., Ding, M., Qin, D., Ren, J., 2016. Spatial and temporal variability of marine-origin matter along a transect from Zhongshan Station to Dome A, Eastern Antarctica. J. Environ. Sci. (China) 46, 190–202. https://doi.org/10.1016/j. jes.2015.07.011.

Lide, D.R., 2005. Abundance of elements in the earth's crust and in the sea. In: Lide, D.R. (Ed.), CRC Handbook of Chemistry and Physics, Internet Version 2005. CRC Press, Boca Raton.

Liu, K., Hou, S., Wu, S., Zhang, W., Zou, X., Pang, H., Yu, J., Jiang, X., Wu, Y., 2019. Dissolved iron concentration in the recent snow of the Lambert Glacial Basin, Antarctica. Atmos. Environ. 196, 44–52.

Liu, K., Hou, S., Wu, S., Zhang, W., Zou, X., Yu, J., Jiang, X., Wu, Y., 2021. Assessment of heavy metal contamination in the atmospheric deposition during 1950–2016 A. D. from a snow pit at Dome A, East Antarctica. Environmental Pollution 268, 115848. https://doi.org/10.1016/j.envpol.2020.115848.

Liu, H., Anwar, S., Fang, L., Chen, L., Xu, W., Xiao, L., Zhong, B., Liu, D., 2022. Source apportionment of agricultural soil heavy metals based on PMF model and multivariate statistical analysis. Environ. Forensics 25 (1–2), 40–48. https://doi.org/10.1080/15275922.2022.2047838.

Marchant, B.P., Saby, N.P.A., Arrouays, D., 2017. A survey of top soil arsenic and mercury concentrations across France. Chemosphere 181, 635–644. https://doi.org/10.1016/j.chemosphere.2017.04.10.

Matsuoka, K., Skoglund, A., Roth, G., de Pomereu, J., Griffiths, H., Headland, R., Herried, B., Katsumata, K., Brocq, A.L., Licht, K., Morgan, F., Neff, P.D., Ritz, C., Scheinert, M., Tamura, T., Putte, A. Van de, van den Broeke, M., von Deschwanden, A., Deschamps-Berger, C., Van Liefferinge, B., Tronstad, S., Melvær, Y., 2021. Quantarctica, an integrated mapping environment for Antarctica, the Southern Ocean, and subantarctic islands. Environ. Model. Softw. 140, 105015.

Norris, G., Duvall, R., Brown, S., Bai, S., 2014. EPA Positive Matrix Factorization (PMF) 5.0 Fundamentals and User Guide. U.S. Environmental Protection Agency, Washington, DC, EPA/600/R-14/108 (NTIS PB2015-105147).

Nyamgerel, Y., Han, Y., Kim, S., Hong, S.-B., Lee, J., Hur, S.D., 2020. Chronological characteristics for snow accumulation on Styx Glacier in northern Victoria Land, Antarctica. J. Glaciol. 66 (260), 916–926. https://doi.org/10.1017/jog.2020.53.

Nyamgerel, Y., Han, Y., Hwang, H., Han, C., Hong, S., Hur, S., Lee, J., 2024. Climate-related variabilities in the Styx-M ice core record from northern Victoria Land, East Antarctica, during 1979–2014. Sci. Tot. Environ. 935, 173319. https://doi.org/10.1016/j.scitotenv.2024.173319.

Planchon, F.A., Boutron, C.F., Barbante, C., Cozzi, G., Gaspari, V., Wolff, E.W., Ferrari, C.P., Cescon, P., 2002. Changes in heavy metals in Antarctic snow from Coats Land since the mid- 19th to the late-20th century. Earth Planet Sci. Lett. 200 (1–2), 207–222.

Rhodes, R.H., Baker, J.A., Millet, M.A., Bertler, N.A.N., 2011. Experimental investigation of the effects of mineral dust on the reproducibility and accuracy of ice core trace element analyses. Chem. Geol. 286 (3–4), 207–221. https://doi.org/10.1016/j.chemgeo.2011.05.006.

Rodenburg, L.A., Meng, Q., Yee, D., Greenfield, B.K., 2014. Evidence for photochemical and microbial debromination of polybrominated diphenyl ether flame retardants in San Francisco Bay sediment. Chemosphere 106, 36–43. https://doi.org/10.1016/j.chemosphere.2013.12.083.

Sayyed, M.R.G., 2014. Lithological control on the mobility of elements during chemical weathering. Comunicações Geológicas 101 (1), 63–69.

Schwanck, F., Simões, J.C., Handley, M., Mayewski, P.A., Auger, J.D., Bernardo, R.T., Aquino, F.R., 2017. A 125-year record of climate and chemistry variability at the Pine Island Glacier ice divide, Antarctica. Cryosphere 11 (4), 1537–1552. https://doi.org/10.5194/tc-11-1537-2017.

Shi, G., Teng, J., Ma, H., Li, Y., Sun, B., 2015. Metals and metalloids in precipitation collected during CHINARE campaign from Shanghai, China, to Zhongshan Station, Antarctica: Spatial variability and source identification. Global Biogeochem. Cycles 29, 760–774. https://doi.org/10.1002/2014GB005060.

Shi, G., Teng, J., Ma, H., Wang, D., Li, Y., 2018. Metals in topsoil in Larsemann Hills, an ice-free area in East Antarctica: lithological and anthropogenic inputs. Catena 160, 41–49. https://doi.org/10.1016/j.catena.2017.09.001.

Taghvaee, S., Sowlat, M.H., Mousavi, A., Hassanvand, M.S., Yunesian, M., Naddafi, K., Sioutas, C., 2018. Source apportionment of ambient PM2.5 in two locations in central Tehran using the Positive Matrix Factorization (PMF) model. Sci. Total Environ. 628–629, 672–686. https://doi.org/10.1016/j.scitotenv.2018.02.096.

Tang, X., Guo, J., Dou, Y., Zhang, Y., Cheng, S., Luo, K., Yu, L., Cui, X., Li, L., Zhang, S., Sun, B., 2020. Glaciological and meteorological conditions at the Chinese Taishan Station, East Antarctica. Front. Earth Sci. 8, 250. https://doi.org/10.3389/feart.2020.00250.

Tuohy, A., Bertler, N., Neff, P., Edwards, R., Emanuelsson, D., Beers, T., Mayewski, P., 2015. Transport and deposition of heavy metals in the Ross Sea Region, Antarctica. J. Geophys. Res. Atmos. 120, 10996–11011. https://doi.org/10.1002/2015JD023293.

Vallelonga, P., Barbante, C., Cozzi, G., Gaspari, V., Candelone, J.-P., Van De Velve, K., Morgan, V.I., Rosman, K.J.R., Boutron, C.F., Cescon, P., 2004. Elemental indicators of natural and anthropogenic aerosol inputs to Law Dome, Antarctica. Ann. Glaciol 39, 169–174. https://doi.org/10.3189/172756404781814483.

Van De Velde, K., Vallelonga, P., Candelone, J.P., Rosman, K., Gaspari, V., Cozzi, G., Barbante, C., Udisti, R., Cescon, P., Boutron, C.F., 2005. Pb isotope record over one century in snow from Victoria Land, Antarctica. Earth Planet. Sci. Lett. 232, 95–108. https://doi.org/10.1016/j.epsl.2005.01.007.

Yang, D., Yao, T., Wu, G., Zhao, H., Zhu, M., Deji Qu, D., Shi, Y., 2024. Identifying the natural and agricultural impacts on the glaciochemistry of the Aru ice core on the northwestern Tibetan Plateau. Sci. Tot. Environ. 906, 167501. https://doi.org/10.1016/j.scitotenv.2023.167501.

Wedepohl, K.H., 1995. The composition of the continental crust. Geochim. Cosmochim. Acta 59, 1217–1232. https://doi.org/10.1016/0016-7037(95)00038-2.

Zheng, K., Li, Y., Li, Z., Huang, J., 2021. Provenance tracing of dust using rare earth elements in recent snow deposited during the pre-monsoon season from mountain glaciers in the central to northern Tibetan Plateau. Environ. Sci. Pollut. Res. 28 (33), 45765–45779. https://doi.org/10.1007/s11356-021-13561-x.

Xiao, C., Allison, I., Ren, J., Qin, D., Zhang, M., Li, Z., 2004. Meteorological and glaciological evidence for different climatic variations on the east and west sides of the Lambert Glacier basin, Antarctica. Ann. Glaciol. 39, 188–194. https://doi.org/10.3189/172756404781814492.

Xu, G., Chen, L., Zhang, M., Zhang, Y., Wang, J., Lin, Q., 2019. Year-round records of bulk aerosol composition over the Zhongshan Station, Coastal East Antarctica. Air Qual. Atmos. Health 12, 271–288. https://doi.org/10.1007/s11869-018-0642-9.

Xu, Q., Chu, Z., Gao, Y., Mei, Y., Yang, Z., Huang, Y., Yang, L., Xie, Z., Sun, L., 2020. Levels, sources and influence mechanisms of heavy metal contamination in topsoils in Mirror Peninsula, East Antarctica. Environmental Pollution 257, 113552. https://doi.org/10.1016/j.envpol.2019.113552.